Numerical study of three-dimensional incompressible thermal flows in complex geometries

Part II: computational studies

Received May 1995
Revised August 1995

Rafael Moreno
Exxon Production Research Company, Houston, Texas, USA, and
Balasubramaniam Ramaswamy
Department of Mechanical and Environmental Engineering, University of California at Santa Barbara, USA

Introduction

Using the three-dimensional iterative Navier-Stokes-Energy equations solver described in part I (Vol. 7 No. 4, pp. 297-343), a series of numerical experiments have been performed in a set of complex three-dimensional geometries of interest. Each of the geometries has its own importance and is of interest for different reasons.

First, a cubic cavity of unit length with two static blocks of equal size symmetrically placed inside as seen in Figure 1 is filled with fluid (Pr = 1.0), static at t = 0. Suddenly, the surface temperature of both blocks changes to θ =10, the surface temperature of the bottom, top, left and right walls of the enclosing cavity becomes θ = 0, and the front and back walls of the enclosing cavity become insulated. The three-dimensional geometry of this problem can be seen in Figure 2.

This problem can be viewed as a coarse approximation to the heat transfer phenomenon that occurs in heat exchangers[1,2]. Also, the problem has practical importance owing to its obvious relation to the cooling of electronic equipment inside computers[3-5]. This is a very interesting domain because it combines many classical problems into one. Both regions A and C share very similar boundary conditions and geometric properties with the benchmark problem described in part I of this study. Saitoh and Hirose[6], de Vahl Davis[7], Le Quéré[8], and many others have analysed such a two-dimensional problem in

Erratum

Please note that in Part I of this article (*HFF*, Vol. 7 No. 4) the names of the authors were inadvertently transposed – the first named author is Rafael Moreno.

International Journal of Numerical Methods for Heat & Fluid Flow
Vol. 7 No. 5, 1997, pp. 497-524.
© MCB University Press, 0961-5539

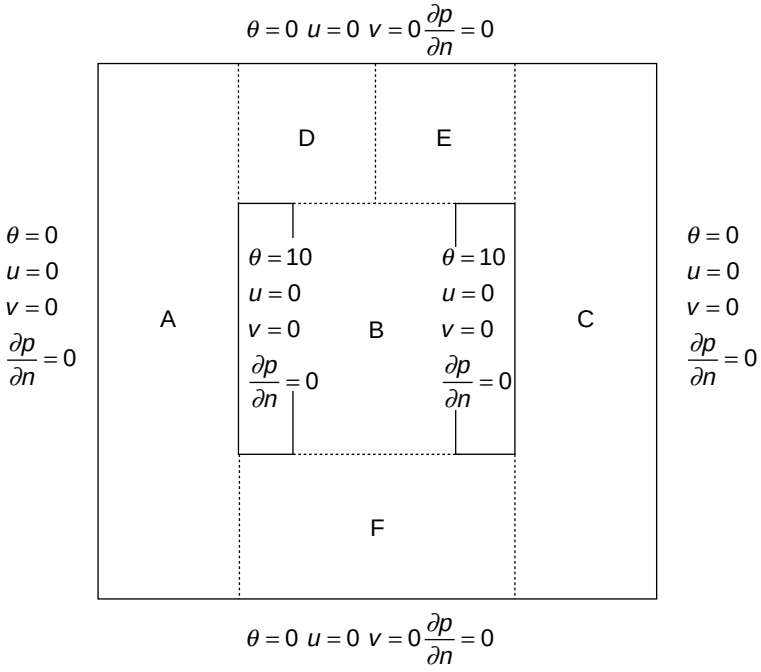

Figure 1.
Geometry for the problem where two internal blocks heated to a constant temperature are surrounded by a containing cavity cooled to a constant temperature on its left, right, top and bottom walls

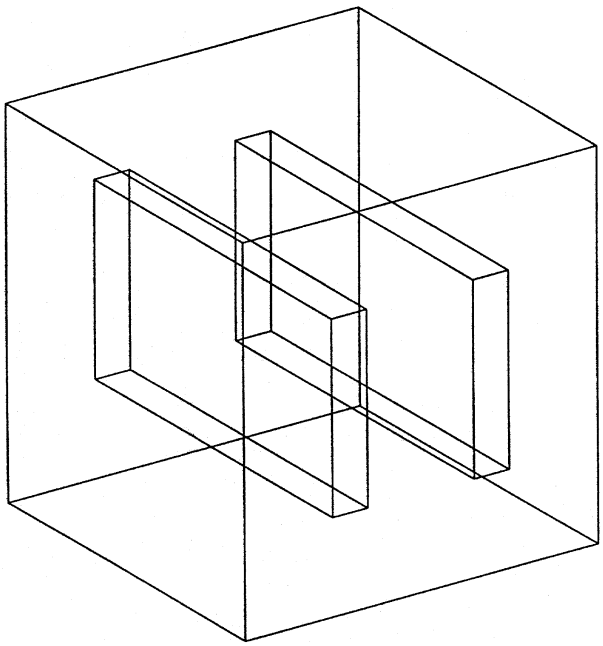

Figure 2.
Geometry for the problem where two internal blocks heated to a constant temperature are surrounded by a containing cavity cooled to a constant temperature on its left, right, top and bottom walls, and insulated on its front and back walls

detail, while Pepper[9], Moreno[10], and Reddy and Reddy[11], among others, have extended the study into three dimensions.

Regions *D* and *E* resemble the problem of heating from the bottom, known as Rayleigh-Bénard convection. Studies such as those by Mukutmoni and Yang[12], Goldhirsch *et al.*[13], Shaw[3], and Pepper[9] explore this type of flow in some detail. Moreover, region *B* resembles the problem of chimney flow. Works such as those by Asako *et al.*[14], Hawkins *et al.*[15], Straatman *et al.*[16], and Al-Alusi and Bushnell[17] are representative.

However, very few works have been published on the interaction of all of these types of flows. It is for that reason that Adlam's[18] two-dimensional simulation of such a problem is an important contribution and why it was decided to broaden the scope of his study by performing numerical experiments over a larger range of Rayleigh numbers, and by extending it into three dimensions. Hence, the two-dimensional and three-dimensional aspects of flows in this geometry have been explored for various Rayleigh numbers between 10^3 and 10^5. Although the grids generated are all regular and there is no refinement near the boundaries of the cavity, the results compare very well with numerical experiments available in the literature.

Second, the motion of fluids across heated interconnected cavities is an important problem, because complex fluid systems can be built using these interconnected cavities as building blocks. For example, the flow of air in a structure[19,20] can be simulated if we can describe the structure in question as a collection of interconnected heated blocks of different sizes. Or the pasteurization process of bottled fluids[21] can be simulated by describing the container as a collection of interconnected blocks of different cross-sectional areas.

An example of the use of the heated parallelepiped as a building block is the two-dimensional problem described by Figure 3 and its three-dimensional version in Figure 4. Two cubic cavities of different dimensions are interconnected as shown. The temperature is then specified at different locations, while the heat flux is specified at others, as described in the same figure.

A number of numerical and experimental studies of similar domains exist in the literature. Ku *et al.*[22] use a pseudospectral method to solve the three-dimensional Navier-Stokes equations for the flow over a backward-facing step and several other geometries[23]. The backward-facing step problem can be viewed as a special case of the geometry we consider. However, they do not consider thermal effects in their study as we do. Similarly, Reddy and Reddy[11] use a penalty finite element approach to solve for the three-dimensional incompressible flow in a square contraction. The domain in question is very similar to the one we concentrate on but it is tilted 90 degrees clockwise, the cavity has a different aspect ratio, thermal effects are not taken into account and different boundary conditions are used. For a detailed study of thermal flows in this kind of geometry, one has to revert to the two-dimensional case. Evren-Selamet *et al.*[24,25] use a fractional step formulation incorporating a second, order Godunov discretization of the convective terms in order to consider a large

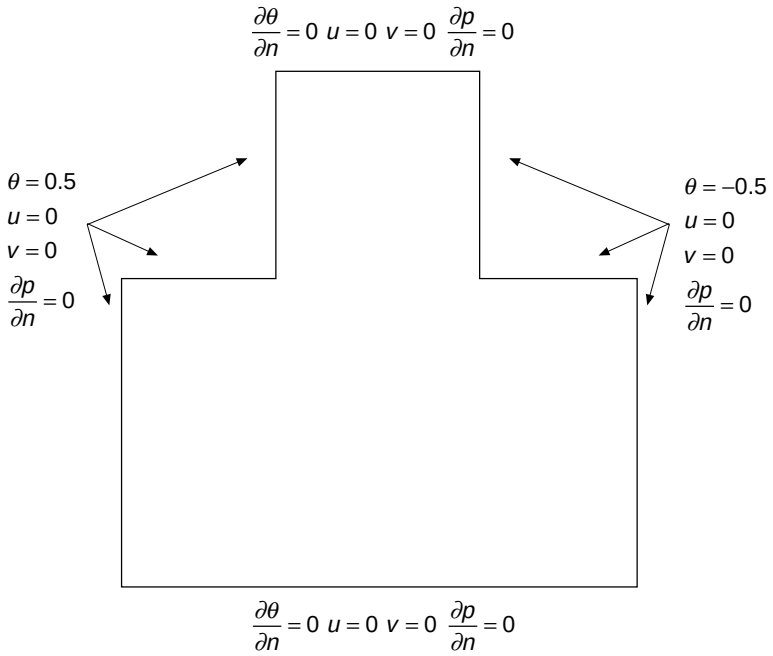

Figure 3.
Geometry for the problem where two cavities of different sizes are interconnected, and the system is heated from the left on both cavities, cooled from the right on both cavities, and insulated on the top and bottom

number of aspect ratios, Rayleigh numbers, Prandtl numbers and Grashof numbers. This paper attempts to extend the work of these researchers and the study of thermal flows in this geometry into three-dimensions and a broader range of boundary and fluid conditions.

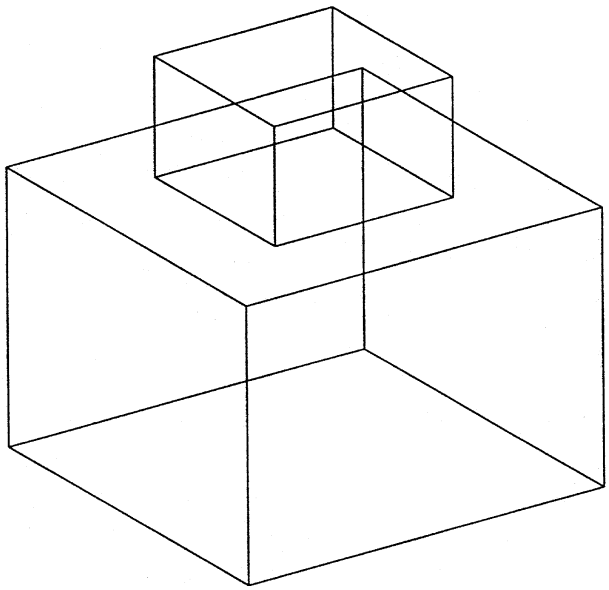

Figure 4.
Geometry for the problem where two cavities of different sizes are interconnected, and the system is heated from the left on both cavities, cooled from the right on both cavities, and insulated on the front, back, top and bottom. The top portion of the bottom cavity is also heated, cooled and insulated in the same manner

Presented here are the simulation results obtained for both the two-dimensional and three-dimensional versions of this problem. In the two-dimensional case, the finest grid used consisted of 41×41 grid points, while in the three-dimensional case, it consisted of $41 \times 41 \times 17$ grid points. These calculations have been performed assuming a Prandtl number of 1.0 for various values of the Rayleigh number between 10^3 and 10^6. For both geometries of interest, all numerical experiments were conducted in a CRAY Y-MP supercomputer and required between one and four hours of CPU time. In all cases, the kinetic energy of the fluid was monitored throughout the simulation. When the kinetic energy of the fluid did not change significantly (by more than 2 or 3 per cent points) in a reasonable amount of time (usually between ten and 20 time steps), the solution was deemed close to the steady state solution. Moreover, for all the cases presented, a grid independence study was performed. For all conditions and Ra numbers, solutions were sought at different mesh resolutions from coarse (11×11 grid points in two dimensions and $11 \times 11 \times 11$ in three dimensions) to fine (41×41 grid points in two dimensions and $41 \times 41 \times 17$ grid points in three dimensions). All solutions presented in this study are such that no significant qualitative changes were observed as the resolution increased.

Problem one: cold cavity with two internal heated bodies

Two-dimensional problem

By comparison with the benchmark problem, a series of properties of the solution can be expected and pointed out a priori. First, the geometry as well as the boundary conditions are symmetric with respect to the $x = 0.5$ line, so the solution is expected to be symmetric with respect to this line as well. Second, the temperature gradient between the hot inner blocks and the cold surrounding cavity is large in comparison to that present in the benchmark problem, where the temperature difference between hot and cold walls was of unit magnitude. As a result, elevated v velocities for the same Ra are expected.

Moreover, certain fluid motions can be expected. Both the region between the left block and the cold left wall of the enclosing cavity, and the region between the right block and the right wall of the enclosing cavity share very similar boundary and geometric properties with the benchmark problem itself. Hence, the formation of a circulation cell in both regions is expected. The region between the two heated blocks is subject to large positive non-dimensional θ temperatures. This will create larger v velocities directed against the gravity gradient, so flow directed upwards is expected in this region. Notice how the two regions between the top wall of both blocks and the top wall of the surrounding cavity resemble the classic problem of Rayleigh-Bérnard convection. It is reasonable then to believe that rotation cells will also form in both these regions. What makes this specific problem interesting is that it is not obvious how all these effects will combine in the cavity, how they will move the fluid within the cavity and how they will enhance or degrade the heat transfer between the internal bodies and the fluid.

Figure 5, together with Tables I and II, summarize the results of the numerical experiments performed. Velocity vector plots have been included to visualize the fluid flow, as well as temperature contour plots to visualize the heat transfer phenomena involved. The tabulated data include the maximum fluid velocities in the *x* and y directions, as well as the minimum, median and maximum Nusselt numbers for every wall in the cavity and the internal bodies for every Rayleigh number explored.

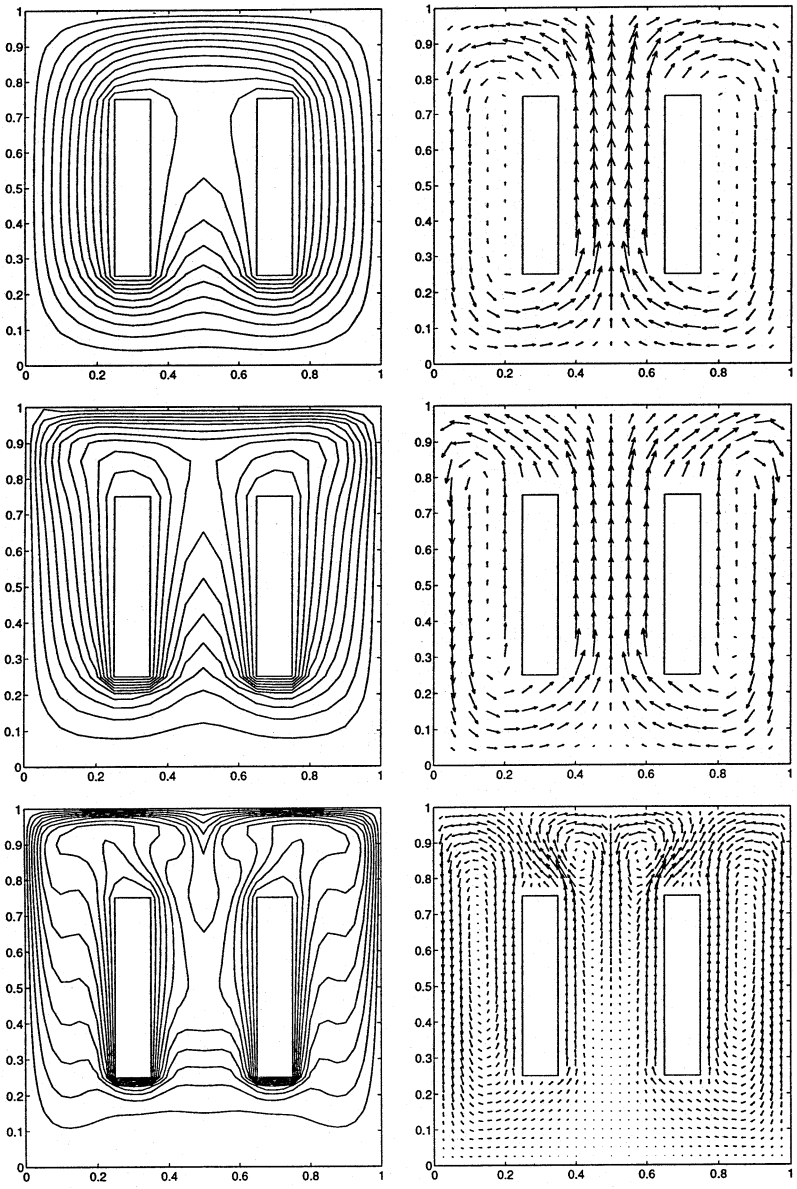

Figure 5.
Temperature contours and vector plots for the two-dimensional problem of a cold cavity with two internal heated bodies (from top to bottom: $Ra = 10^3$, $Ra = 10^4$, $Ra = 10^5$)

Unknown	Ra 10^3	10^4	10^5
u_{max}	8.6850	39.7546	133.7345
v_{max}	20.8847	57.2681	259.9340
Cavity's left wall			
Nu_0	–27.1018	–38.6544	–63.9388
Nu_{max}	–36.0416	–71.7945	–142.6654
Nu_{min}	0.0000	0.0000	0.0000
Cavity's right wall			
Nu_0	27.1023	38.5705	63.9393
Nu_{max}	36.0583	70.1761	142.6665
Nu_{min}	0.0000	0.0000	0.0000
Cavity's top wall			
Nu_0	40.9772	107.2169	193.7386
Nu_{max}	59.5684	115.5602	247.9880
Nu_{min}	0.0000	0.0000	0.0000
Cavity's bottom wall			
Nu_0	–17.5672	–8.2928	–5.0390
Nu_{max}	–21.1617	–10.3218	–6.7731
Nu_{min}	0.0000	0.0000	0.0000

Table I.
Important numerical results of the simulation of the two-dimensional problem of the cavity with internal heated bodies

Unknown	Ra 10^3	10^4	10^5
Block's left wall			
Nu_0	–48.1395	–50.4387	–110.6531
Nu_{max}	–75.6368	–109.8182	–248.6765
Nu_{min}	–45.7400	–39.4148	–64.3757
Block's right wall			
Nu_0	20.6089	50.2810	81.1948
Nu_{max}	67.2966	105.1971	210.2952
Nu_{min}	14.7814	34.2702	68.4978
Block's top wall			
Nu_0	36.4911	15.2904	21.9310
Nu_{max}	51.0695	18.7599	43.7806
Nu_{min}	31.6920	10.7688	13.9864
Block's bottom wall			
Nu_0	–84.6488	–131.3487	–251.0902
Nu_{max}	–84.7026	–145.4591	–294.7911
Nu_{min}	–77.7713	–131.1712	–237.7013

Table II.
Important numerical results of the simulation of the two-dimensional problem of the cavity with internal heated bodies

In order to better describe the behaviour of the fluid system, let us divide the domain into six different regions *A* to *F* as described in Figure 1. This decomposition into regions is introduced purely to facilitate the descriptions of the interesting phenomena observed as the Rayleigh number is increased.

At low *Ra*, the fluid motion can be described as follows. Fluid penetrates region *B* from the bottom of the cavity. It rises along the $x = 0.5$ symmetry line and splits left and right near the top of the cavity. The fluid then moves over the heated blocks in regions *D* and *E* and penetrates regions *A* and *C* from the top as it moves downward into region *F*. Once in *F*, the fluid moves under the heated blocks and enters region *B* to complete one cycle of circulation. In addition, even at low *Ra*, a counterclockwise rotating cell forms in region *A* and, owing to the symmetry of the problem, a clockwise rotating cell also forms in region *C*.

Nonetheless, as the *Ra* increases drastic changes in the flow pattern can be observed. First, the rotation cells in regions *A* and *C* become better defined and stronger, in the sense that the fluid velocities involved increase in magnitude. Moreover, the centre of rotation of the cell moves away from the heated block wall towards the centre of the region and the cell elongates in the *y* direction. Second, a clockwise rotating cell forms in region *D* together with a counter-clockwise rotating cell in region *E*, both near the $x = 0.5$ line. These cells force a change in the direction of flow in region *B*. The fluid near the block walls in this region still moves upwards, against the gravity gradient owing to the strong buoyant force. However, when these additional rotation cells appear, flow near the $x = 0.5$ line is reversed, and can penetrate region *B* from the top as far as the $y = 0.30$ line when the Rayleigh number is 10^5. Finally, the relative magnitude of the flow velocity in region *F* progressively decreases as the *Ra* increases, especially in the neighbourhood of the $x = 0.5$ line, in comparison with the magnitude of the flow velocity in the rest of the cavity. All these changes are interesting because, in combination, they drastically change the heat transfer behaviour of the system.

The maximum Nusselt number can be found at the bottom of both heated blocks. It is in this region where the temperature gradient is largest and, thus, where thermal energy is most readily lost. In particular, the top wall of the enclosing cavity also presents a large Nusselt number. Although these two aspects of the system are important, the overall effect is also interesting. It is clear from the numerical experiments that as the *Ra* increases the heat transfer in most walls of the system studied is enhanced. The isotherm patterns obtained, as well as the numerical values presented, support this conclusion. Hot spots in the fluid, which lead to poor heat flow from the hot bodies inside the cubic cavity become less prominent as the Rayleigh number increases. Moreover, region *B* experiences the most change. At a $Ra = 10^3$ almost the whole region has the same temperature, very close to that of the hot blocks. As the *Ra* increases, the temperature distribution in the region changes and heat flow is enhanced.

Adlam[18] has worked on the same two-dimensional problem for various Rayleigh numbers. Both qualitative and quantitative agreement is observed

between his and the results of this study. He has also simulated the flow around not only two, but four internally heated blocks oriented both horizontally and vertically. Although the simulation in this study was not extended from two to four internal bodies, the simulation was extended from two to three dimensions and a larger range of Rayleigh numbers.

Three-dimensional problem

In the three-dimensional scenario, the geometric arrangement and the boundary conditions are symmetric with respect to both the yz plane at $x = 0.5$, and the yx plane at $z = 0.5$. The solution is expected to be symmetric with respect to these planes. For every Ra, the yx cross-section at $z = 0.5$ is almost identical to the solution of the analogue two-dimensional problem. One can recognize that the two-dimensional problem is the same as the three-dimensional problem when the z dimension is infinite, i.e. the front and back walls are infinitely apart. It can also be expected that the closer the fluid is to the insulated back and front walls, the smaller the magnitude of the fluid velocities will be, owing to the imposed no-slip boundary condition, thus reducing the intensity of convective heat transfer near the insulated walls.

The numerical experiments suggest that the nature and location of the rotation cells observed in the two-dimensional case do not change as the problem is extended into three dimensions. However, it is certainly true that these cells present three-dimensional aspects not detectable in the two-dimensional simulations. It is also true that these three-dimensional effects gain strength as the Rayleigh number increases.

The three-dimensional aspects of the flow will therefore be concentrated on, that is, the differences rather than the similarities between the two- and three-dimensional flows.

First, let us extend the regions in Figure 1 backwards in the z direction to render them three-dimensional. At $Ra = 10^3$, three-dimensional effects are concentrated in regions D and E. Instead of purely rolling about the z axis, the rotation cells in both regions move fluid three-dimensionally from regions B, D and E into A and C.

At $Ra = 10^4$, these three-dimensional motions persist. In addition, a new rolling motion around the x axis can be observed across the domain. However, in other regions of the domain three-dimensional effects are negligible. It is important to notice how the fluid velocities have increased by a factor of four to six, and how the temperature distribution at steady state has changed. At this Rayleigh number, it is clear that the heat transfer has been enhanced mostly in region B, where at lower Rayleigh numbers the temperature was mostly uniform. In addition, the heat transfer has been affected in regions D and E. The new rolling motion about the x axis, previously described, traps some fluid in regions D and E near the top of the heat-generating blocks, allowing it to heat up and, hence, reduce the heat transfer in the region. Surprisingly, this adverse effect creates a larger temperature gradient close to the top wall of the enclosing cavity, thus enhancing heat loss there.

At $Ra = 10^5$, the three-dimensional effects observed at $Ra = 10^4$ have intensified, and a set of new flow features can be described. In particular, three-dimensional effects that were previously limited to regions *D* and *E* can be observed in regions *A*, *B* and *C*. Near the *xz* plane that splits these regions into two equal parts, new rotation cells about the *x* axis can be found. These new effects move fluid particles away from the insulated front and back walls of the enclosing cavity towards the central *yx* symmetry plane. Here, the rotational cells observed in the two-dimensional simulations dominate and basically distribute the fluid around the domain. Some will be trapped in the strong cells in regions *D* and E, while some will be forced towards the insulated walls to begin a new cycle. At this Rayleigh number, the heat transfer is greatly enhanced in regions *A*, *B* and *C*, where the local *Nu* has doubled or even tripled, while the heat flow near the top of the heated blocks has again decreased. It is concluded that the fact that fluid in this region lies between two strong counter-rotating cells prevents the crucial mixing required for effective convection of heat.

Some of these effects can be observed in Figures 6-10, while they are quantified in Tables III and IV.

Problem two: two heated and interconnected cavities of different sizes

Two-dimensional problem

In the two-dimensional version of this problem, two rectangular cavities of different sizes are placed one on top of the other. In detail, a square cavity of 0.4×0.4 square units is centred on top of a rectangular cavity of 1.0×0.6 square units, such that the distance from the top left-hand corner of the bottom block to the bottom left-hand corner of the top block is exactly 0.3 units. These cavities are discretized in a regular fashion such that the distance between grid points is $\Delta x = 1/40$ units in the *x* direction and $\Delta y = 1/40$ units in the *y* direction.

When the block-to-block interface is removed, an irregular cavity is left which can be easily discretized with a regularly spaced grid. The cavity is differentially heated, that is, the left walls of both the bottom and top blocks are heated to a constant temperature ($\theta = 0.5$), while the right walls of both blocks are cooled to a constant temperature ($\theta = -0.5$). At the same time, the top wall of the top block and the bottom wall of the bottom block are insulated. The remaining segment to the left of the top cavity is heated ($\theta = 0.5$), while the remaining segment to the right of the top cavity is cooled ($\theta = -0.5$).

In contrast with the problem of the square cavity with two heated blocks, although there is geometric symmetry with respect to the $x = 0.5$ line, the solution will not be symmetric owing to the differences in boundary conditions across the cavity. However, notice how both cavities are subjected to the same conditions observed in the benchmark problem. For this reason, the overall solution is expected to be an unknown combination of the benchmark solutions for each of the blocks.

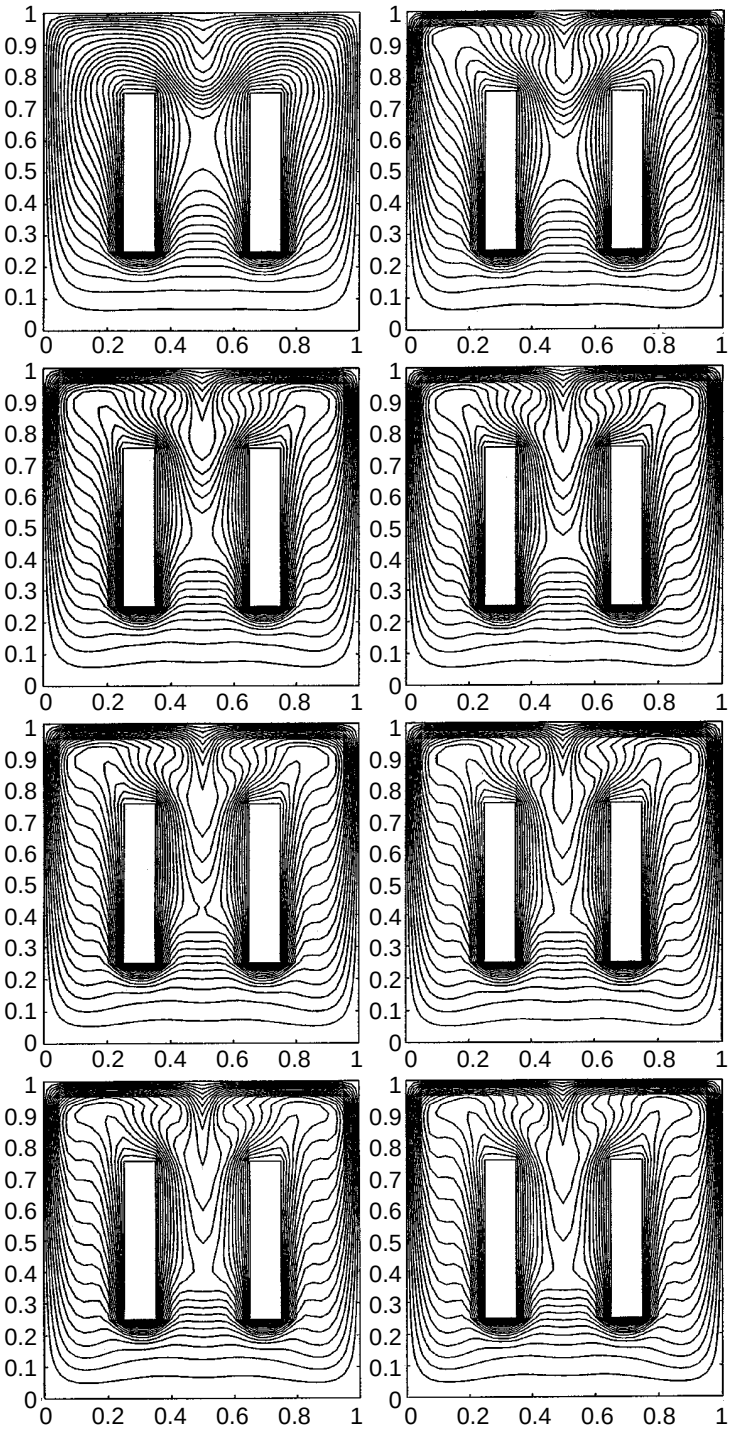

Figure 6.
Temperature contours for $Ra = 10^5$ at different yx cross-sections (from top left to bottom right z = 0.0625, 0.1250, 0.1875, 0.2500, 0.3125, 0.3750, 0.4375, 0.5000)

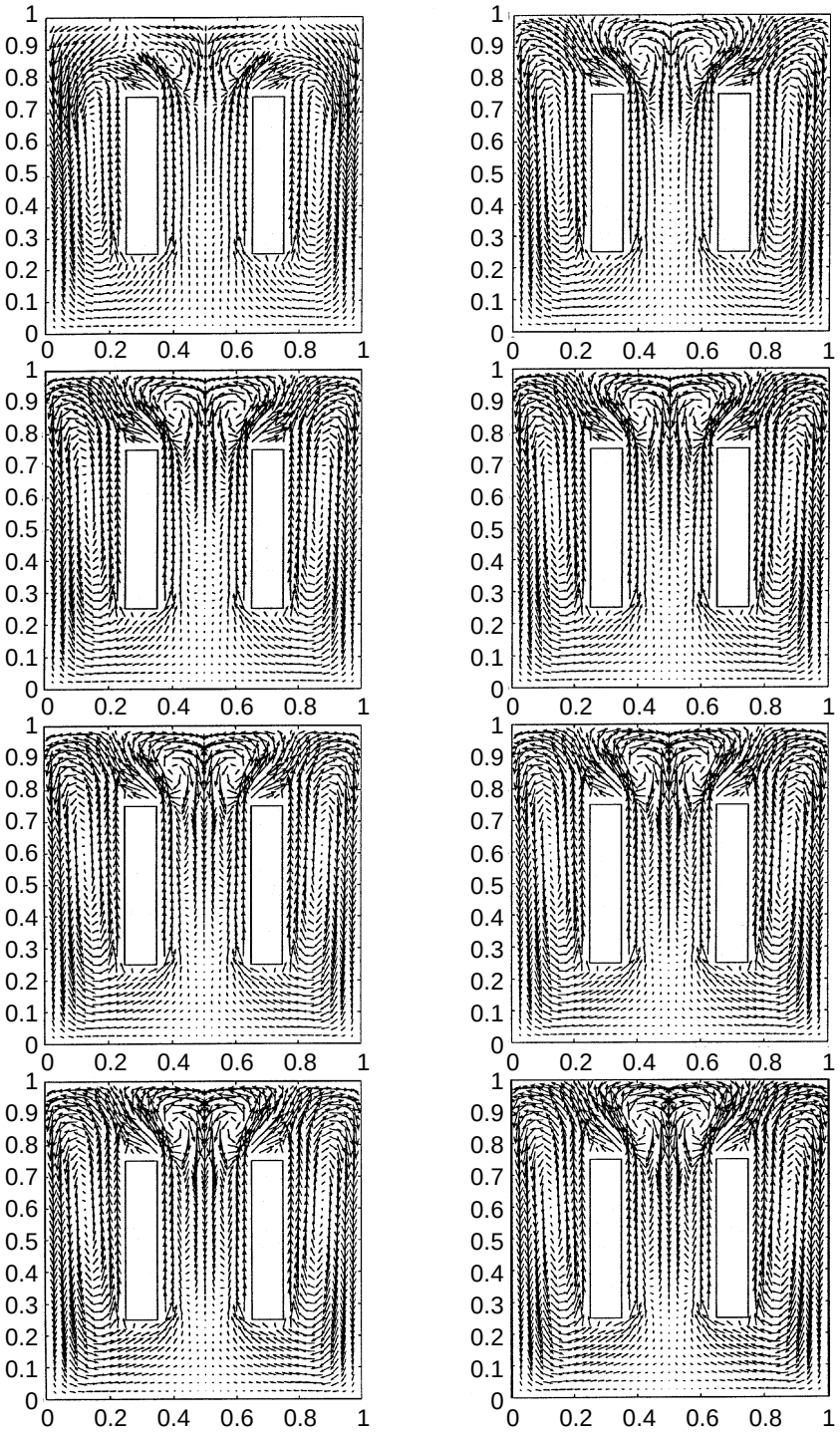

Figure 7.
Vector plots for $Ra = 10^5$ at different yx cross-sections (from top left to bottom right z = 0.0625, 0.1250, 0.1875, 0.2500, 0.3125, 0.3750, 0.4375, 0.5000)

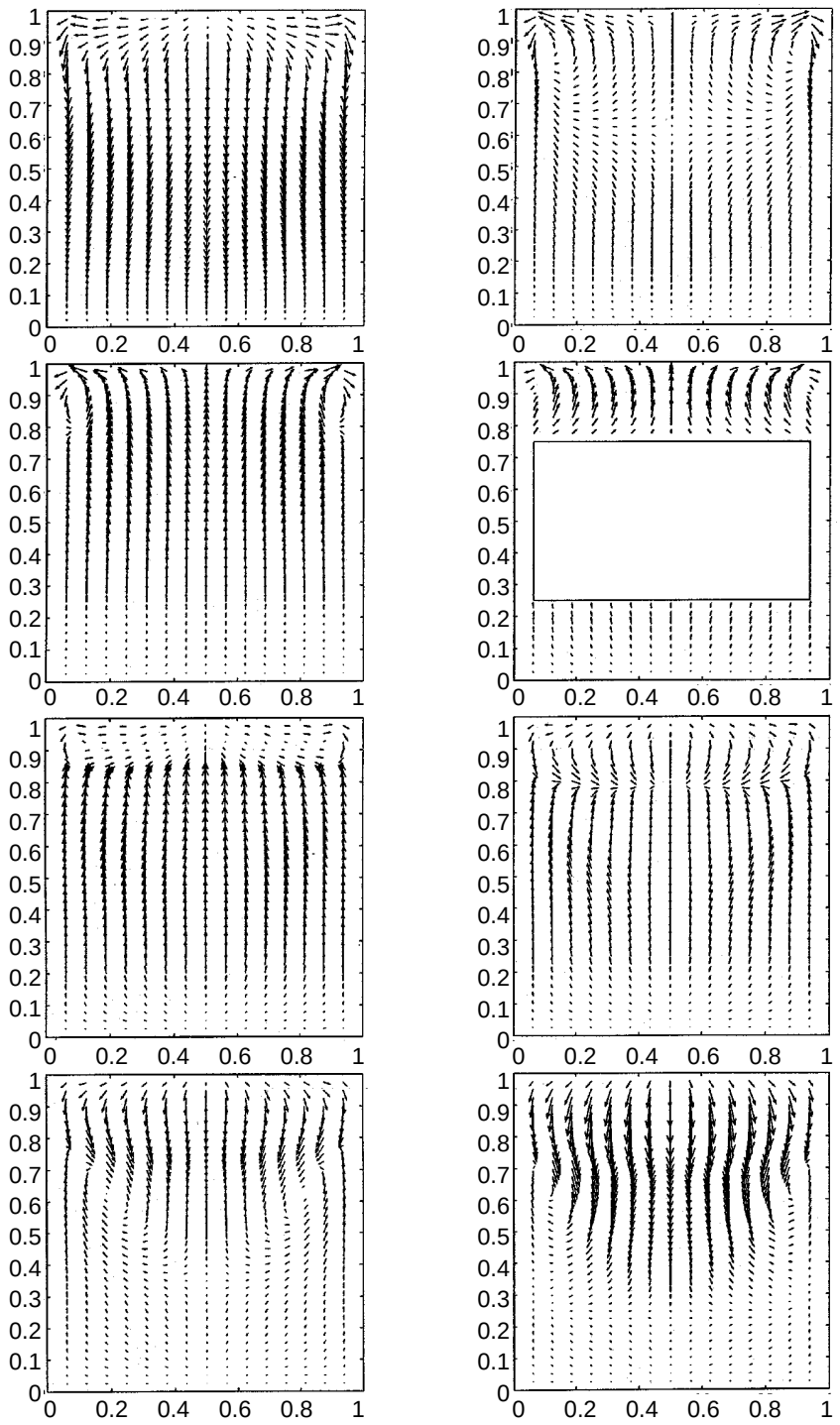

Figure 8.
Vector plots for $Ra = 10^5$ at different yz cross-sections (from top left to bottom right x = 0.0750, 0.1250, 0.1750, 0.3000, 04000, 0.4250, 0.4500, 0.5000)

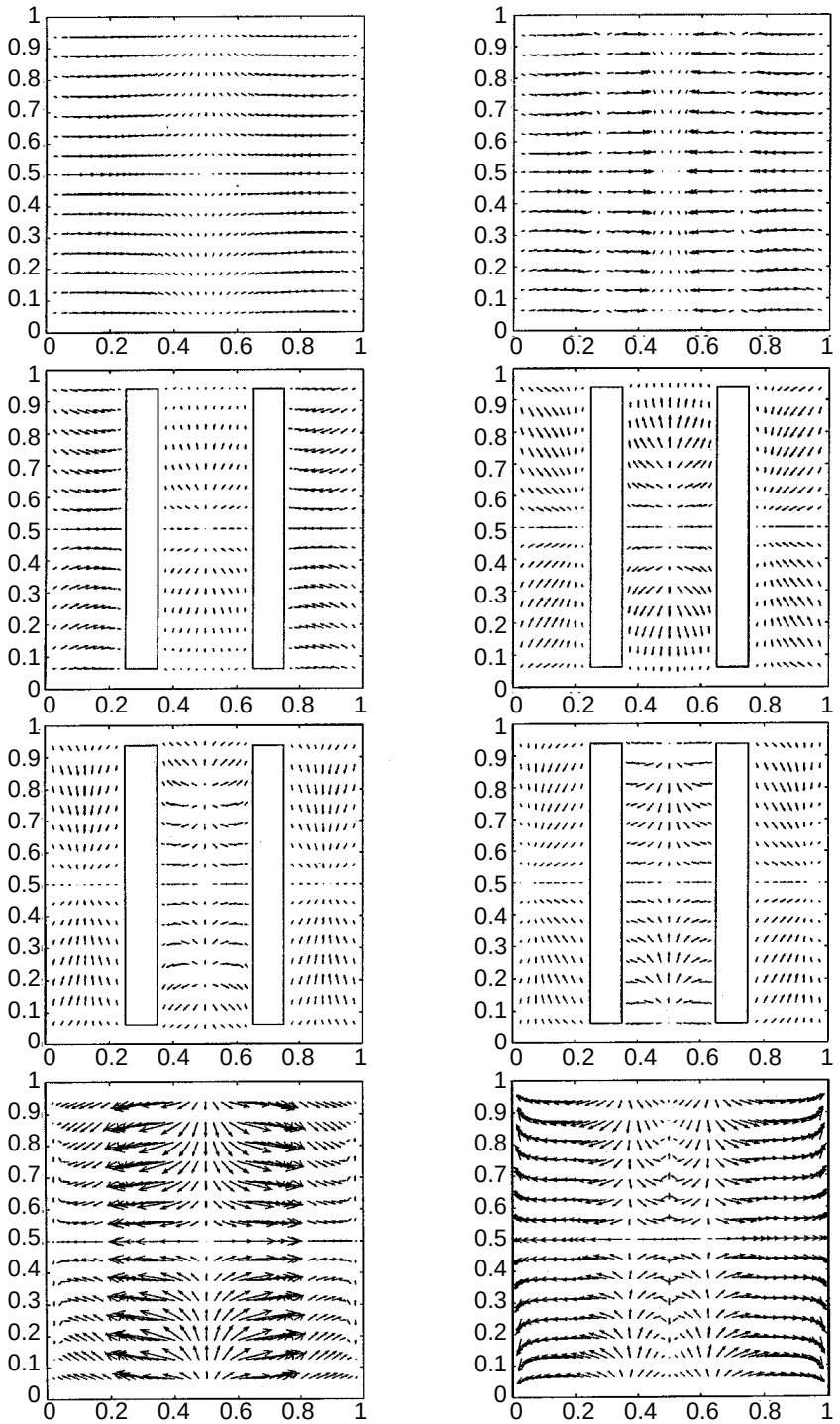

Figure 9.
Vector plots for $Ra = 10^5$ at different zx cross-sections (from top left to bottom right y = 0.0500, 0.2250, 0.3500, 0.5000, 0.6000, 0.6750, 0.7750, 0.8750)

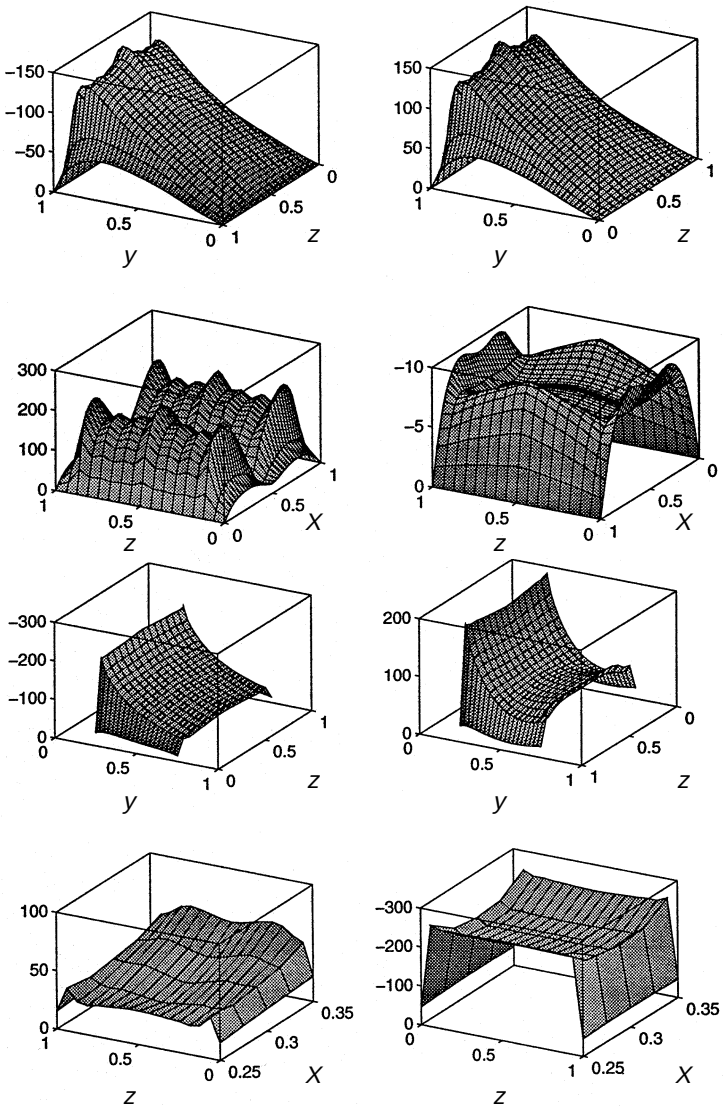

Figure 10.
Nusselt number surfaces for the internal heated bodies problem at $Ra = 10^5$. (From top left to bottom right: left wall, right wall, top wall and bottom wall of enclosing cavity, left wall, right wall, top wall and bottom wall of heated block)

Figure 11 is a collection of isotherm patterns and velocity vector plots of the numerical solution of the two-dimensional version of this problem at various Rayleigh numbers. For low Rayleigh numbers between 10^3 and 10^4, a dominant v velocity in the y direction is observed near the heated walls in both the top and bottom cavities. It can be seen that a circulation cell has formed and is centred close to the centre point of the bottom cavity. It can also be observed that the effect of the circulation cell extends into the top cavity. In it, the flow enters the interface near the bottom left corner of the top cavity, moves close to the left wall,

turns right near the top left corner until it reaches the top right corner, turns right again and follows the left wall until it leaves through the interface near the bottom right-hand corner of the top cavity. Owing to the no-slip condition, all the fluid velocities diminish as the fluid approaches the system boundaries.

For these low *Ra*, the isotherms in the top cavity are mainly parallel to each other, indicating that the main heat transfer mechanism in the region is conduction. A change will be observed from conductive to convective heat transfer in the region in question as the *Ra* increases, owing to the increase in the magnitude of the buoyancy term in the *y*-momentum equation. Another interesting fact is that the isotherms are nearly perpendicular to the interface between the two heated blocks. This indicates that the heat flux at the interface is almost zero. A change will be noticed in this behaviour as well. With respect to the bottom cavity, it can be observed that the isotherms are curved, especially near the top left and top right corners. This is an indication of convective heat transfer in action. Nevertheless, the curvature of the isotherms is not pronounced. The isotherm curvature can be used as a measure of the intensity of convective heat transfer. An increase is expected in the isotherm curvature as the *Ra* increases. It is interesting to notice that, even in the presence of an additional region full of fluid, the temperature contour pattern in the bottom cavity is very similar to that observed in the two-dimensional benchmark

Table III. Important numerical results of the simulation of the three-dimensional problem of the cavity with internal heated bodies

Unknown	*Ra* 10^3	10^4	10^5
u_{max}	10.7350	42.0180	146.3050
v_{max}	20.3288	74.7820	259.7574
w_{max}	2.9010	19.1087	75.2839
Cavity's left wall			
Nu_0	–28.9099	–38.1771	–65.1947
Nu_{max}	–38.4019	–56.2517	–149.1987
Nu_{min}	0.0000	0.0000	0.0000
Cavity's right wall			
Nu_0	28.9099	38.1771	65.1947
Nu_{max}	38.4019	56.2512	149.1991
Nu_{min}	0.0000	0.0000	0.0000
Cavity's top wall			
Nu_0	35.9753	57.2146	136.6531
Nu_{max}	59.1149	124.9805	216.9999
Nu_{min}	0.0000	0.0000	0.0000
Cavity's bottom wall			
Nu_0	–21.5739	–11.6334	–6.7294
Nu_{max}	–25.1210	–16.8746	–9.4115
Nu_{min}	0.0000	0.0000	0.0000

Unknown	Ra 10^3	10^4	10^5
Block's left wall			
Nu_0	–45.6476	–43.3403	–93.8591
Nu_{max}	–75.9551	–95.9861	–225.7839
Nu_{min}	–20.5397	–19.3242	–14.6539
Block's right wall			
Nu_0	14.2900	44.3693	70.4122
Nu_{max}	59.8298	96.3870	196.2367
Nu_{min}	–1.4143	2.0602	14.4599
Block's top wall			
Nu_0	38.3017	19.6896	34.1396
Nu_{max}	66.8484	56.6772	61.2042
Nu_{min}	21.4135	15.6943	15.2040
Block's bottom wall			
Nu_0	–74.3842	–110.2744	–200.8954
Nu_{max}	–81.6641	–126.9324	–260.7970
Nu_{min}	–24.2493	–27.8494	–45.6382

Table IV. Important numerical results of the simulation of the three-dimensional problem of the cavity with internal heated bodies

problem for the same Rayleigh number. Even at these low Rayleigh numbers, it is clear that heat is most readily lost by the cold right wall of the top cavity, as evidenced in Table V.

From the nature of the problem, one might expect the formation of a circulation cell in the top cavity also. The boundary conditions are very similar to those for the bottom cavity, so why has a circulation cell not formed in the region? This study has only worked with a specific aspect ratio between the top and bottom cavities for different values of the Rayleigh number. Nevertheless, Evren-Selamet[25] has worked with different aspect ratios, Rayleigh numbers and Prandtl numbers as well and, when his data are examined, it appears that the formation of the cell in the smallest cavity is dependent on both the aspect ratio, the Ra and the Pr. Our choice of Pr and aspect ratio seems to preclude the formation of a circulation cell in the region.

As previously expressed, as the Ra increases, changes in the flow and the heat transfer phenomena are observed. The heat flow through the cold right wall of the top cavity increases steadily, as well as that of the hot left wall of the bottom cavity. In fact, the local median Nusselt number increases by a factor of between seven and ten, as the Ra varies between 10^3 and 10^6. Other than that, the maximum fluid velocities steadily increase throughout the domain. No rotation cell is observed to form in the top cavity, while the cell in the bottom cavity elongates in the x direction as it did in the two-dimensional benchmark problem until, at $Ra = 10^6$, the initially well-formed rotation cell in the centre of the bottom cavity splits into two, less organized rotation cells. The most dramatic change is, however, the obvious transition from mostly conductive to

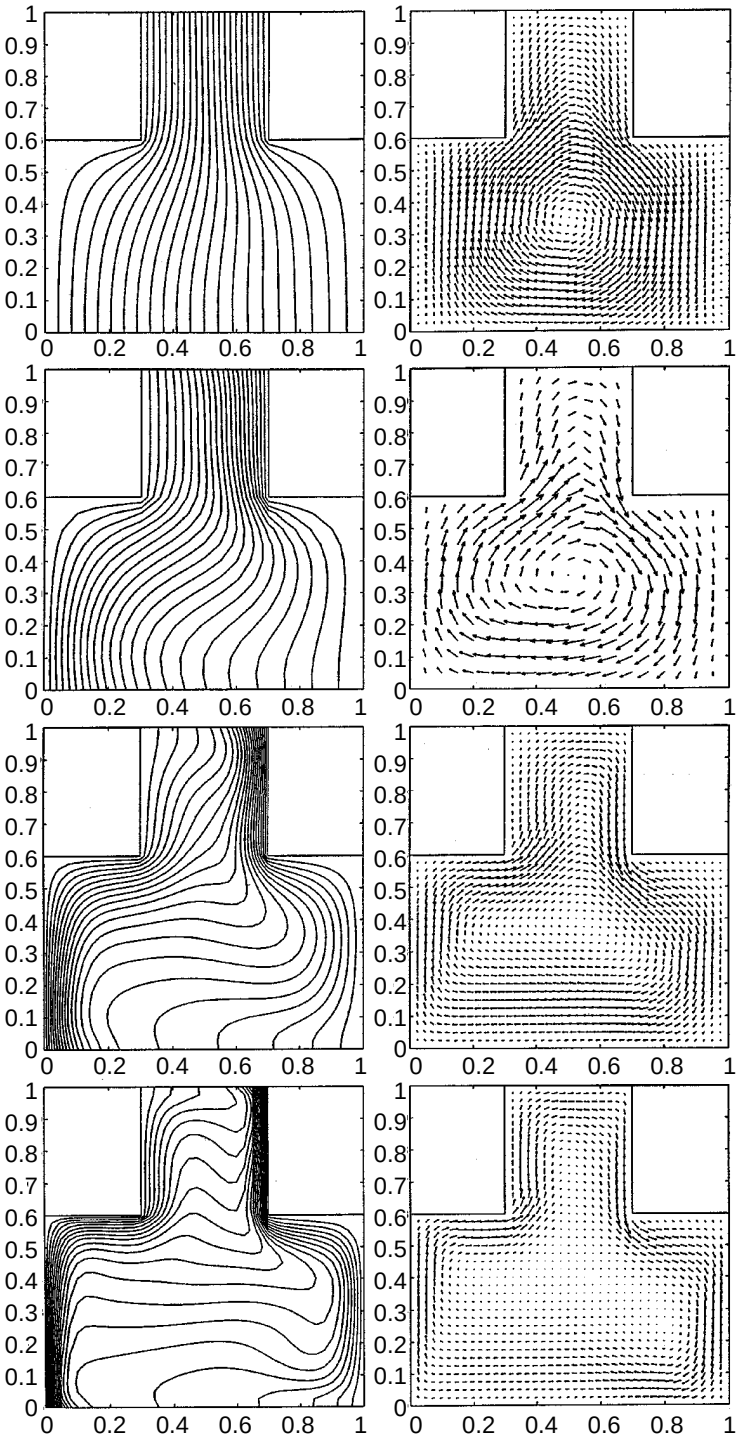

Figure 11.
Temperature contours and vector plots for the two-dimensional problem of two interconnected cavities (from top to bottom: $Ra = 10^3$, $Ra = 10^4$, $Ra = 10^5$, $Ra = 10^6$)

Unknown	10^3	Ra 10^4	10^5	10^6
u_{max}	1.7392	14.3952	66.1818	197.8826
v_{max}	2.1761	12.6104	59.7307	203.5376
Bottom cavity's hot left wall				
Nu_0	0.9201	2.0012	5.7983	11.0567
Nu_{max}	1.0955	2.4918	7.3071	15.1915
Nu_{min}	0.0000	0.0000	0.0000	0.0000
Bottom cavity's hot left top wall				
Nu_0	–0.7845	–1.3384	–3.1998	–7.2396
Nu_{max}	–3.2069	–2.9324	–5.4084	–8.8265
Nu_{min}	0.0000	0.0000	0.0000	0.0000
Top cavity's hot left wall				
Nu_0	2.3761	1.7295	1.6761	3.4765
Nu_{max}	3.6512	2.5459	4.0510	5.5477
Nu_{min}	2.3539	1.6689	0.8786	1.1993
Top cavity's cold right wall				
Nu_0	2.7204	3.7210	7.9446	14.3236
Nu_{max}	4.2729	5.2669	9.1219	18.2384
Nu_{min}	2.6265	3.3693	6.7546	12.0839
Bottom cavity's cold right top wall				
Nu_0	0.6920	0.8176	1.6527	1.9957
Nu_{max}	3.5031	3.6341	6.0228	6.6965
Nu_{min}	0.0000	0.0000	0.0000	0.0000
Bottom cavity's cold right wall				
Nu_0	0.7845	0.6038	1.3377	3.4196
Nu_{max}	0.8449	0.7681	2.0760	4.8417
Nu_{min}	0.0000	0.0000	0.0000	0.0000

Table V.
Important numerical results of the two-dimensional version of the problem where two parallelepiped cavities of different sizes are differentially heated while interconnected

mostly convective heat transfer in both cavities. This is clear from the curved isotherm pattern and the temperature distribution (see Figures 12 and 13). In addition, an increase in heat transfer across the interface between two blocks is of interest. The effects observed in this region lead to the conclusion that at low Ra one could treat the top cavity and the bottom cavity almost as two independent heat transfer problems by replacing the open interface by an insulated wall. However, as the Rayleigh number increases, this simplification becomes unreasonable and one must treat both cavities as a unit.

Three-dimensional problem

It is important to recognize the relation of both the two-dimensional and three-dimensional problems in order to understand both the similarities and the

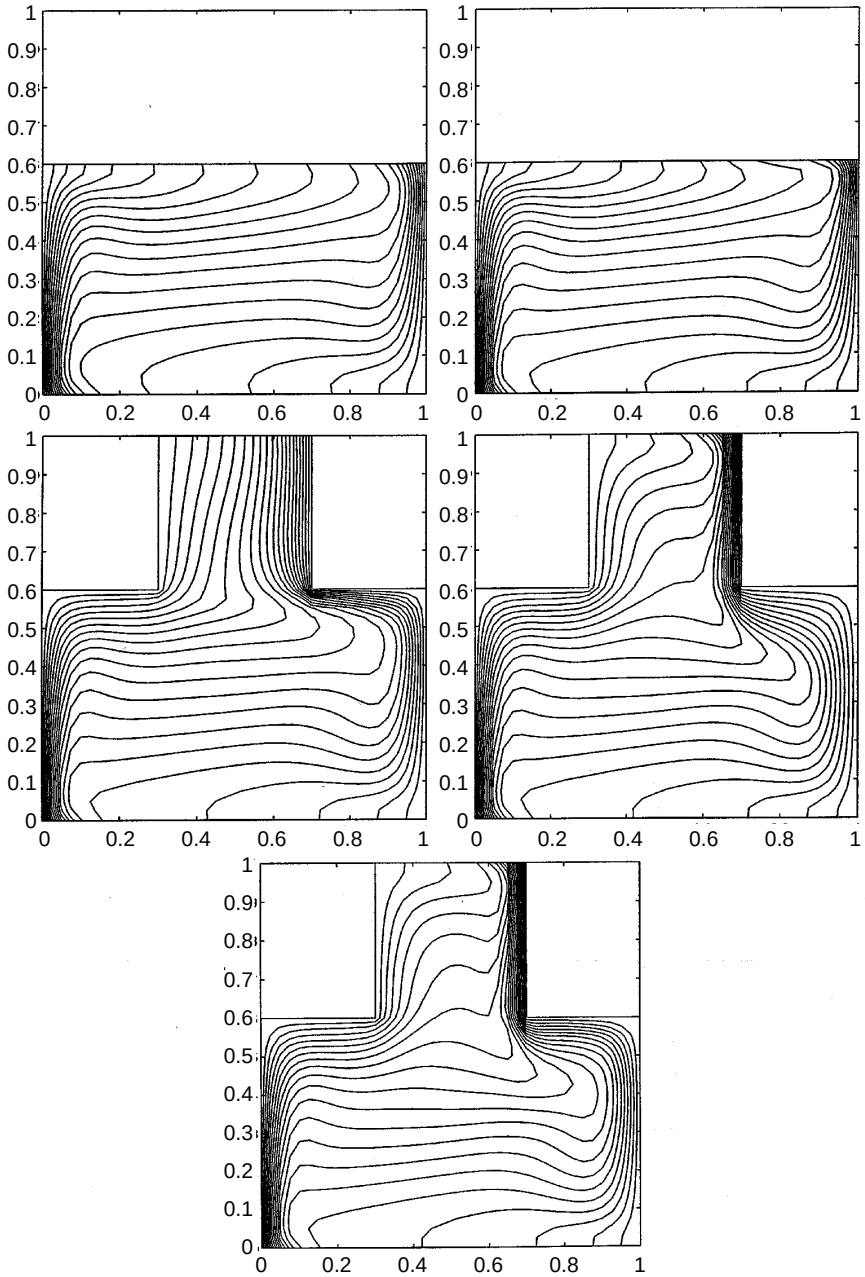

Figure 12.
Temperature contours or isotherms for $Ra = 10^6$ at different yx cross-sections (from top left to bottom right z = 0.1000, 0.2000, 0.3000, 0.4000, 0.5000)

differences between both versions of the same problem. The two-dimensional problem can be viewed as the corresponding three-dimensional problem where the front and back walls of both interconnected blocks are located at infinity. Owing to that fact, the solutions of the two-dimensional problem for a specific

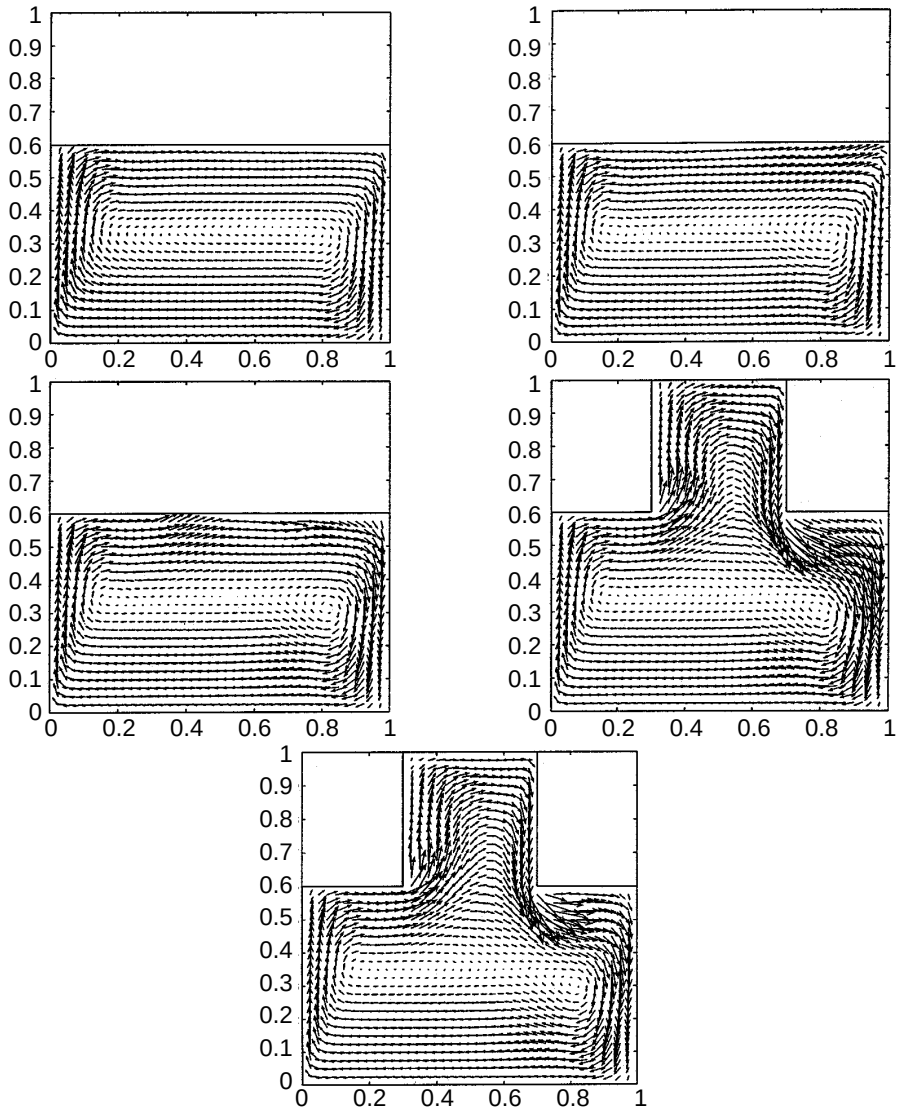

Figure 13. Vector plots for $Ra = 10^6$ at different yx cross-sections (from top left to bottom right z = 0.1000, 0.2000, 0.3000, 0.4000, 0.5000)

Ra were expected to be very similar to that of the three-dimensional problem at the yx cross-section at $z = 0.5$ for the same Ra. On the other hand, the three-dimensional solution at yx cross-sections will differ from the two-dimensional solution the closer it is to the front and back walls of the irregular cavity.

As with the benchmark problem, as the Ra increases, an increase is expected in the fluid velocities, and a progressively more important role played by the w velocity in the z direction. This increase in velocity has been observed together

with an increase in heat flux near the heated walls, hence a larger local *Nu* is expected as the *Ra* increases.

At low Rayleigh numbers (i.e. 10^3, 10^4), the three-dimensional effects are concentrated mostly near the front and back walls of the lower cavity and near the two-block interface. These effects are also stronger in the region between the *yz* planes at $x = 0.4$ and $x = 0.6$. In this three-dimensional region of the bottom cavity, fluid near the front and back walls is forced towards the centre of the cavity as if a weak three-dimensional circulation cell is being formed. In addition, the fluid is also forced in and out of the smaller upper cavity by sudden contraction and expansion, generating larger than average velocities.

At a Rayleigh number of 10^5, the fluid flow pattern is more interesting. The circulation cell along the *z* axis centred in the bottom cavity elongates in the *x* direction as in the two-dimensional case. It is is now so strong that some of the fluid particles near its centre will only flow in the bottom cavity. Concurrently, a larger irregular rotational cell encompasses the first one. Fluid close to the system boundaries penetrates the top cavity from the left and exits it from the right. However, no independent rotational cell is observed in the top cavity. As in the two-dimensional case, formation of such an independent cell seems to be directly related to the aspect ratio between both cavities[25]. Our choice of aspect ratio seems to preclude such a formation even at large Rayleigh numbers.

As with lower *Ra*, the fluid accelerates as it moves from the larger bottom cavity to the smaller top cavity. This effect is three-dimensional owing to the geometric structure of the domain (i.e. the three-dimensional domain in question is not merely a projection of the two-dimensional one along the *z* axis, but represents a similar but different environment). The weak three-dimensional effects near the front and back walls still force fluid away from these walls and towards the centre of the cavity, where the two-dimensional effects take over and force the particles either to flow inside the bottom cavity or travel back and forth between the bottom and top cavities. It is only at larger Rayleigh numbers that a change in this flow pattern is clearly visible.

At $Ra = 10^6$, the same circulation cells observed at $Ra = 10^5$ rotating along the *z* axis are still present but have gained intensity. The sudden contraction and expansion of the fluid penetrating and exiting the top cavity still cause the strongest three-dimensional effects in the domain. However, in contrast with the flow pattern observed at lower Rayleigh numbers, strong three-dimensional effects such as circulation cells can be observed in the vicinity of the two-block interface, especially near the regions where the fluid penetrates the top cavity and even more so in the region where the fluid suddenly expands as it leaves the top cavity into the bottom one. As can be seen in Figure 14, the sudden expansion of fluid leaving the top cavity creates a reversal of flow in its vicinity, and as a result, a set of two three-dimensional rotational cells is formed. These cells extend in the *x* direction from $x = 0.6$ to $x = 0.95$. Their effect can also be seen in Figure 15. Notice how the three-dimensional effects of the sudden expansion of the flow from the top cavity to the bottom one are clearly observed near the left wall of the bottom cavity. In contrast, notice how the effects of the

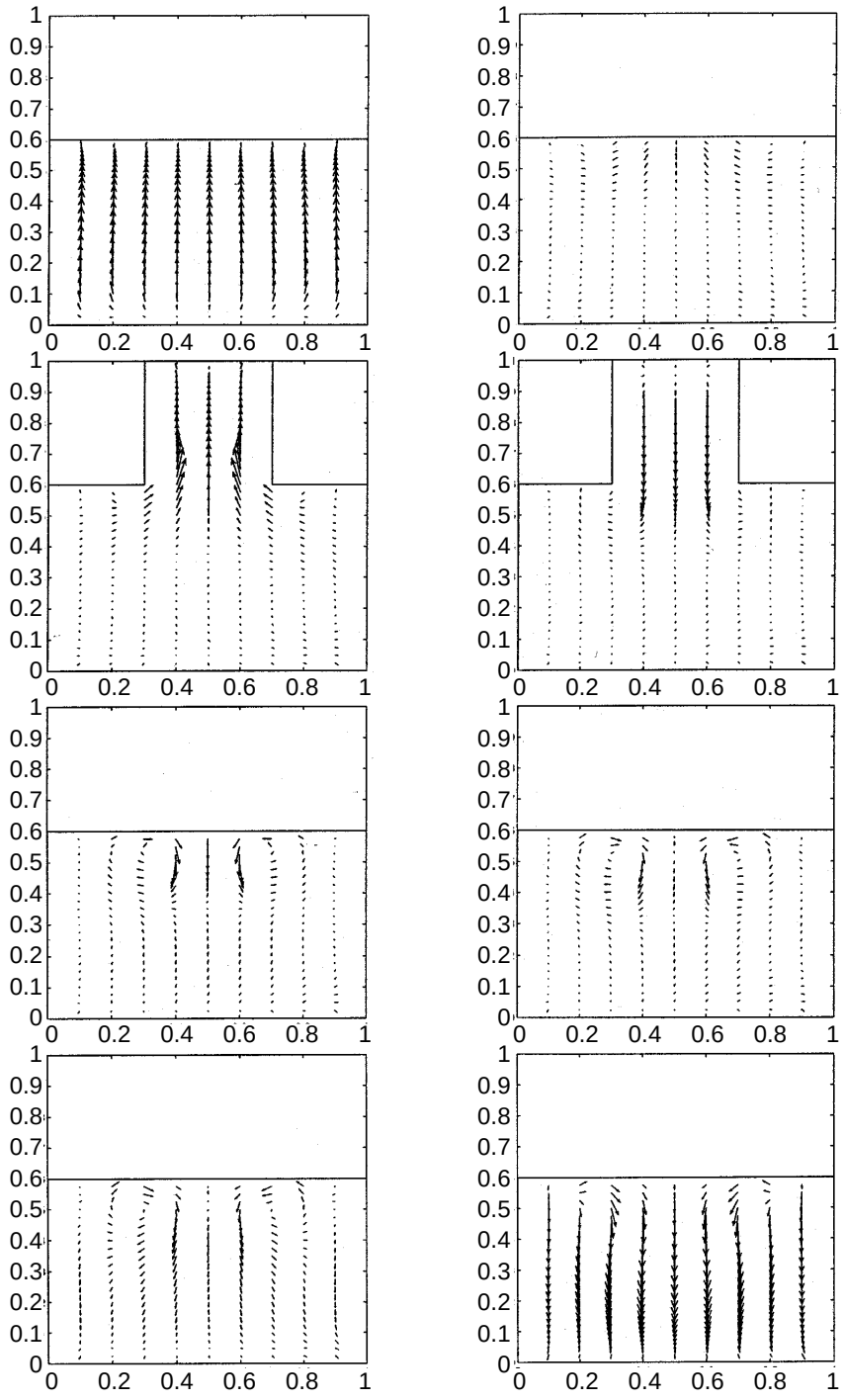

Figure 14. Vector plots for $Ra = 10^6$ at different yz cross-sections (from top left to bottom right x = 0.0500, 0.0275, 0.3750, 0.6250, 0.7250, 0.8000, 0.8500, 0.9500)

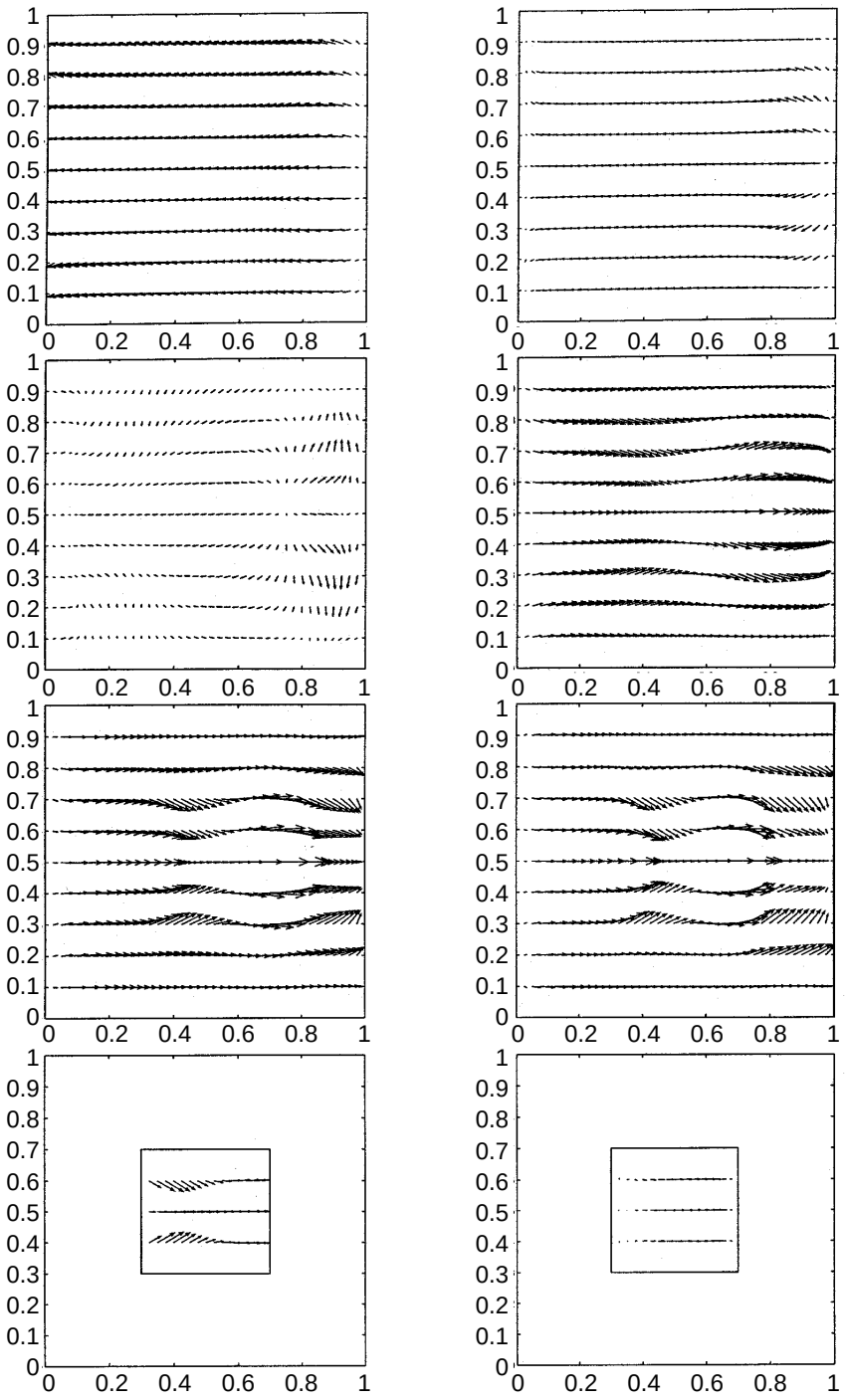

Figure 15.
Vector plots for $Ra = 10^6$ at different zx cross-sections (from top left to bottom right y = 0.0500, 0.0225, 0.3250, 0.4750, 0.5500, 0.5750, 0.62500, 0.7250)

sudden contraction of the flow from the bottom cavity to the top one are mostly localized in the region next to the left wall of the top cavity. In both cases, notice how the three-dimensional effects become negligible as we approach the insulated bottom face of the bottom cavity and the insulated top face of the top cavity. These observations are a final indication that the three-dimensional effects in the particular domain of two interconnected cavities of different sizes are a result of the sudden expansion and sudden contraction which the enclosed fluid experiences.

What is the impact of these three-dimensional motions in the way heat is transferred in the cavity? The major effect is that the circulation cells formed in the bottom cavity owing to the sudden expansion help the convective process such that the Nusselt number near the top right corner of the bottom cavity is three times larger in the three-dimensional case than the Nusselt number in the same region in the two-dimensional case (see Figure 16). This is clearly a significant heat transfer enhancement which can be directly attributed to the three-dimensional aspects of the flow. It is also evident after examining Table VI that as the Rayleigh number increases, the local Nusselt number values generally increase.

In Evren-Selamet *et al.*'s paper[24] and in Evren-Selamet's doctoral dissertation[25] the problem of buoyancy-driven flow inside an irregular two-dimensional cavity is thoroughly studied for different aspect ratios and different values of both the Rayleigh number and the Prandtl number. Our two-dimensional results are for an aspect ratio not treated in their study. Nevertheless, there is no qualitative discrepancy between our results and theirs

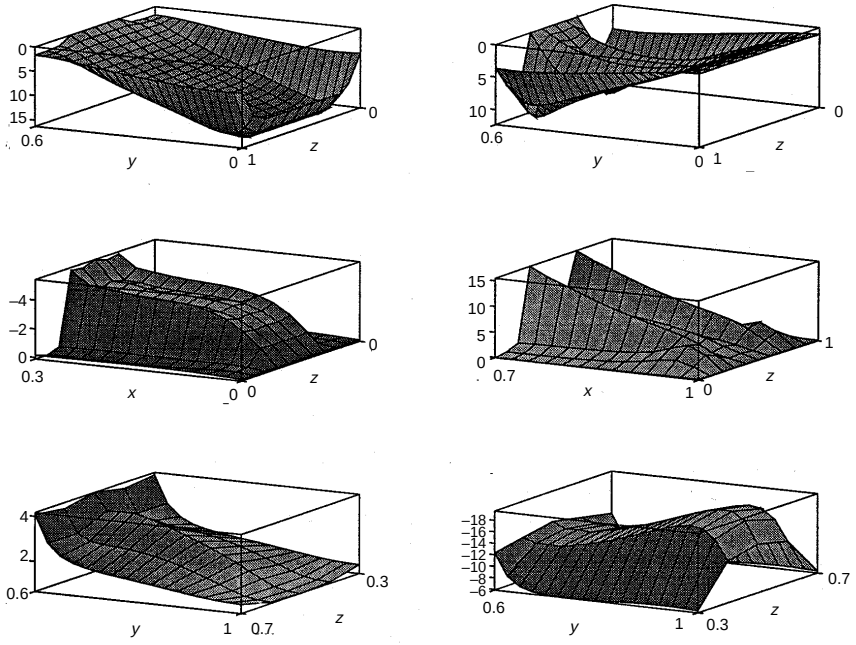

Figure 16.
Nusselt number surfaces for the irregular cavity problem at $Ra = 10^6$. (From top left to bottom right: left wall of bottom cavity, right wall of bottom cavity, left portion of top wall of bottom cavity, right portion of top wall of bottom cavity, left wall of top cavity and right wall of top cavity)

in terms of the fluid behaviour in the cavity. In fact, some test simulations were performed on exactly the same aspect ratio which they described, but with a much coarser mesh and a slightly larger Prandtl number (Pr = 1.0 instead of Pr = 0.71). The only difference between this study's approach and theirs is that their formulation seems to introduce some artificial diffusion, resulting in an overall smoothing of the steady state solution. Finally, the extension of the problem to three-dimensions has been found to be straightforward and computationally feasible with the current computer resources available.

Concluding remarks

The study presented here concerning the fluid motion and the heat transfer phenomena present in three-dimensional flows in complex geometries leads to

Unknown	Ra 10^3	10^4	10^5	10^6
u_{max}	1.9775	14.9898	56.8450	196.1168
v_{max}	2.2192	11.6043	54.7735	190.0148
w_{max}	0.6284	3.2433	11.5250	49.0390
Bottom cavity's hot left wall				
Nu_0	0.9374	1.6409	5.0564	10.5800
Nu_{max}	1.0767	2.3462	7.0479	16.2553
Nu_{min}	0.0000	0.0000	0.0000	0.0000
Bottom cavity's cold right wall				
Nu_0	0.8190	0.7518	2.1417	4.6855
Nu_{max}	0.9028	1.0388	3.7062	12.2888
Nu_{min}	0.0000	0.0000	0.0000	0.0000
Bottom cavity's hot left top wall				
Nu_0	–0.2716	–0.3763	–0.4059	–0.2009
Nu_{max}	–1.9770	–2.0712	–3.1454	–5.4183
Nu_{min}	0.0000	0.0000	0.0242	0.1076
Bottom cavity's cold right top wall				
Nu_0	0.2577	0.4872	1.7557	1.5311
Nu_{max}	2.0348	3.1508	7.4138	15.4721
Nu_{min}	0.0000	0.0000	0.0000	–0.0765
Top cavity's hot left wall				
Nu_0	2.4103	1.8333	1.3282	2.0542
Nu_{max}	2.8277	2.3306	2.6743	4.1665
Nu_{min}	2.3594	1.5698	0.8723	0.6757
Top cavity's cold right wall				
Nu_0	–2.6657	–3.2981	–7.0156	–14.5328
Nu_{max}	–3.1127	–5.0498	–8.8226	–19.5933
Nu_{min}	–2.5506	–2.7999	–4.4344	–5.8716

Table VI. Important numerical results of the three-dimensional version of the problem where two parallelepiped cavities of different sizes are differentially heated while interconnected

certain conclusions regarding some of their general properties as well as some of the properties of the solution scheme:

- At low Rayleigh numbers, two-dimensional motions dominate, three-dimensional motions are almost negligible and conduction is the dominating heat transfer mechanism.
- As the Rayleigh number increases, the momentum transfer in the *y*-direction increases, leading to an increase in the magnitude of all fluid velocities, an increase in the importance of the three-dimensional motions and a transition from conductive to convective heat transfer.
- In regions where three-dimensional aspects of the flow become more pronounced as the Rayleigh number increases, heat transfer is generally enhanced as observed by comparing the values of the local Nusselt number at different *Ra* and between the two and three-dimensional cases.
- Although the formation of new rotational cells in the flow is enhanced by the increase in Rayleigh number, a direct connection between rotational cell formation and cavity aspect ratios also seems to exist.
- Use of a generalized point successive over-relaxation (PSOR) iterative scheme allows use of the same solver for all the governing equations and a variety of boundary conditions, making the code more readable, compact and general.
- The PSOR iterative scheme allows for good vectorization in the CRAY Y-MP environment as well as for excellent control of convergence and error criteria.
- As expected, the solution of the elliptic pressure equation is the most time-consuming operation in the simulator. In fact, the cost of solving the pressure equation is strongly problem dependent. It was decided to solve for the pressure at every time step at the expense of more computational time required, even when other possible approaches were available.

References

1. Ebadian, M.A., Modest, M.F. and Lavine, A., *Advances in Heat Exchanger Design, Radiation, and Combustion – Conference Proceedings of the 1991 Winter Annual Meeting of the American Society of Mechanical Engineers*, Vol. 182, 1991.
2. Mitra, N.K., Bastani, A. and Fiebig, M., "Numerical simulation of 3D periodically fully developed flow between fins of compact fin-tube heat exchanger", *Advances in Heat Exchanger Design, Radiation, and Combustion – 1991 Winter Annual Meeting of the American Society of Mechanical Engineers*, Vol. 182, 1991, pp. 37-41.
3. Shaw, H., "Laminar mixed convection heat transfer in three-dimensional horizontal channel with a heated bottom", *Numerical Heat Transfer,* Part A, Vol. 23, pp. 445-61, 1993.
4. Garimella, S.V. and Eibeck, P.A., "Onset of transition in the flow over a three-dimensional array of rectangular obstacles", *Thermal Modeling and Design of Electronic Systems and Devices – Winter Annual Meeting of the American Society of Mechanical Engineers,* Vol. 153 No. 1, 1990, pp. 1-6.
5. Manno, V.P. and Azar, K., "Thermal-fluid interactions of neighbouring components on air-cooled circuit boards", *Journal of Electronic Packaging*, Vol. 113 No. 4, 1991, pp. 374-81.

6. Saitoh, T. and Hirose, K., "High-accuracy bench mark solutions to natural convection in a square cavity", *Computational Mechanics*, Vol. 4, 1989, pp. 417-27.
7. de Vahl Davis, G., "Natural convection of air in a square cavity: a bench mark numerical solution", *International Journal for Numerical Methods in Fluids*, Vol. 3, 1983, pp. 249-64.
8. Le Quéré, P., "Accurate solutions to the square thermally driven cavity at high Rayleigh number", *Computers and Fluids,* Vol. 20 No. 1, 1991, pp. 29-41.
9. Pepper, D.W., "Modelling of three-dimensional natural convection with a time-split finite-element technique", *Numerical Heat Transfer*, 1987, Vol. 11, pp. 31-55.
10. Moreno, R., "Numerical study of three-dimensional incompressible thermal flows in complex geometries", Master's thesis, Rice University, 1994.
11. Reddy, M.P. and Reddy, J.N., "Penalty finite element analysis of incompressible flows using element by element solution algorithms", *Computer Methods in Applied Mechanics and Engineering*, Vol. 100, 1992, pp. 169-205.
12. Mukutmoni, D. and Yang, K.T., "Wavenumber selection for Rayleigh-Bénard convection in a small aspect ration box", *International Journal of Heat Mass Transfer*, Vol. 35, 1992, pp. 2145-21.
13. Goldhirsch, I., Pelz, R.B. and Orszag, S.A., "Numerical simulation of thermal convection in a two-dimensional finite box", *Journal of Fluid Mechanics,* Vol. 199, 1989, pp. 1-28.
14. Asako, Y., Nakamura, H. and Faghri, M., "Natural convection in a vertical heated tube attached to a thermally insulated chimney of a different diameter", *Heat Transfer in Convective Flows – 1989 National Heat Transfer Conference*, Vol. 107, 1989, pp. 299-304.
15. Hawkins, L.E., Khan, J.A. and Yao, G., "Numerical solution of buoyancy-driven flow through small openings between two enclosures", *Natural Convection in Enclosures – 28th National Heat Transfer Conference and Exhibition,* Vol. 198, 1992, pp. 105-12.
16. Straatman, A.G., Tarasuk, J.D. and Floryan, J.M., "Heat transfer enhancement from vertical, isothermal channel generated by the chimney effect", *Journal of Heat Transfer,* Vol. 115 No. 2, 1993, pp. 395-402.
17. Al-Alusi, T.R. and Bushnell, D.J., "Experimental study of free convection heat transfer from an array of three horizontal cylinders parallel to a vertical wall", *Journal of Heat Transfer,* Vol. 114 No. 2, 1992, pp. 394-400.
18. Adlam, J.H., "Computation of two-dimensional time-dependent natural convection in a cavity where there are internal bodies", *Computational Fluids*, 1986, Vol. 14, pp. 141-57.
19. Schaelin, A., van der Maas, J. and Moser, A., "Simulation of airflow through large openings in buildings", *ASHRAE Winter Meeting – ASHRAE Transactions*,Vol. 98 pt. 2, 1992, pp. 319-28.
20. Fang, J.B. and Grot, R.A., "Numerical simulation of the performance of building ventilation systems", *1990 Annual Meeting of the American Society of Heating, Refrigerating and Air-Conditioning Engineers – ASHRAE Transactions,* pt. Vol. 2, 1990, pp. 361-6.
21. Lambert, N.J., "Fluid analysis", in Brauer, J.R. (Ed.), *What Every Engineer Should Know about Finite Element Analysis,* Marcel Dekker Inc., New York and Basel, 1988, pp. 177-96.
22. Ku, H.C., Hirsh, R.S., Taylor, T.D. and Rosenberg, A.P., "A pseudospectral matrix element method for solution of three-dimensional incompressible flows and its parallel implementation", *Journal of Computational Physics*, Vol. 82 No. 2, 1989, pp. 260-91.
23. Ku, H.C., Hirsh, R.S. and Taylor, T.D., "A pseudospectral method for solution of the three-dimensional incompressible Navier-Stokes equations", *Journal of Computational Physics,* Vol. 70, 1987, pp. 439-62.
24. Evren-Selamet, E., Arpaci, V.S. and Borgnakke, C., "Simulation of laminar buoyancy-driven flows in an enclosure", *Numerical Heat Transfer,* Part A, Vol. 22, 1992, pp. 401-20.
25. Evren-Selamet, E., "Simulation of laminar buoyancy-driven flows in an enclosure", Doctoral dissertation, University of Michigan, 1991.